Automatica 183 (2026) 112568

Contents lists available at ScienceDirect

Automatica

journal homepage: www.elsevier.com/locate/automatica

Brief Paper

State estimation for lithium-ion batteries based on electrolyte–electrode PDE observers ☆

Sara Sepasiahooyi, Shu-Xia Tang *

Department of Mechanical Engineering, Texas Tech University, TX, United States of America

ARTICLE INFO

Article history:
Received 15 July 2024
Received in revised form 14 May 2025
Accepted 1 August 2025
Available online 9 September 2025

Keywords:
Lithium-ion batteries
State estimation
State-of-Charge
PDE backstepping
Sensitivity analysis

ABSTRACT

Accurate information about the states of an electrochemical battery model facilitates a deeper understanding of battery behavior and enables performance enhancement. This paper first proposes backstepping Partial Differential Equation (PDE) observers for lithium concentration in the electrolyte phase within the negative electrode, positive electrode, and separator. Reverse sensitivity analysis is conducted to identify the most suitable measurable parameter for obtaining the electrolyte lithium concentration at the boundaries, which is used in the design of the electrolyte-phase observer. Subsequently, enhanced observers for the solid-phase lithium concentration in the negative and positive electrodes are developed. The proposed solid-phase observer enables more accurate State-of-Charge (SoC) estimation by leveraging the closed-loop electrolyte-phase observer. Simulations of the reverse sensitivity analysis and state observers are performed on a commercial cylindrical lithium iron phosphate ($LiFePO_4$) cell to validate the effectiveness of the proposed approach.

1. Introduction

1.1. Motivation

As lithium-ion batteries become increasingly integrated into daily life, ensuring their reliable operation is crucial. Accurate knowledge of their internal electrochemical states is essential for understanding their behavior and preventing potential faults to ensure safe operation (Zhang, Couto, & Moura, 2020). However, due to the complexity of battery systems, directly measuring lithium concentration is impractical without specialized laboratory settings (Moura, Chaturvedi, & Krstić, 2014). This necessitates the development of electrochemical state estimation algorithms, which are vital for determining key metrics in battery management systems, such as SoC (Tang, Camacho-Solorio, Wang, & Krstic, 2017).

1.2. Reverse sensitivity analysis algorithms

Sensitivity analysis examines how variations in target parameters contribute to uncertainty in a specific model parameter. It identifies which parameters have the most and least significant impact on the parameter of interest (Alipour, Yin, Tavallaey, Andersson, & Brandell, 2023). Schmidt, Bitzer, Imre, and Guzzella (2010) proposed a novel battery model based on the Fisher information matrix method. Their results facilitate the design of a minimal number of experiments sufficient to fully parameterize the model. Alipour et al. (2023) employed an electrochemical-thermal aging model to perform sensitivity analysis and determine the impact of parameter uncertainties on battery voltage, temperature, and aging. In Lai et al. (2020), an analytical approach was used to conduct sensitivity analysis and determine the voltage sensitivity of the battery to its electrochemical parameters.

A novel class of sensitivity analysis, known as reverse sensitivity analysis, has been introduced in Pesenti, Millossovich, and Tsanakas (2019). It is termed "reverse" because it monitors changes in the target parameter instead of the parameter of interest (Pesenti, 2022). In this study, a reverse sensitivity analysis is conducted to identify the most suitable battery measurement for obtaining the electrolyte lithium concentration at the boundaries, given the complexity of forward sensitivity.

1.3. Estimation algorithms

The state estimation approaches can be categorized into two main groups: data-based and model-based methods. Data-based methods utilize datasets to train artificial intelligence or machine learning models, even in the absence of extensive battery knowledge (Jafari & Byun, 2024). Model-based methods employ

☆ The material in this paper was partially presented at the 63rd IEEE Conference on Decision and Control (CDC), December 16–19, 2024, Milan, Italy. This paper was recommended for publication in revised form by Associate Editor Mamadou Diagne under the direction of Editor Miroslav Krstic.

* Corresponding author.
E-mail addresses: ssepasia@ttu.edu (S. Sepasiahooyi), shuxia.tang@ttu.edu (S.-X. Tang).

https://doi.org/10.1016/j.automatica.2025.112568

various types of battery models to estimate states and performance metrics (Ferreira & Tang, 2025a). SoC estimation from solid-phase lithium concentration is well studied in the literature. In Moura et al. (2014), the lithium concentration in the solid phase within the Single Particle Model (SPM) has been estimated using a linear observer. A backstepping PDE observer is designed by injecting the boundary state error. Subsequently, a combined estimation algorithm has been employed to estimate SoC and State-of-Health. In Tang et al. (2017), a thermal–electrochemical model is introduced to estimate the SoC while considering temperature effects. In Zhang et al. (2020), local observability has been investigated for an SPM incorporating solid-phase dynamics using Kalman decomposition approach. Subsequently, a converged state observer is proposed for the observable subsystem corresponding to the surface lithium concentration in the solid phase.

Besides estimating electrode-level properties, analyzing electrolyte concentration can provide valuable insights into battery states; however, this aspect has received limited attention in existing studies. In Moura, Argomedo, Klein, Mirtabatabaei, and Krstic (2016), the Single Particle Model with electrolyte (SPMe) is introduced to describe lithium concentration in both the solid and electrolyte phases. Additionally, an open-loop observer is designed to estimate lithium concentration in the electrolyte phase. In Zhang, Park, Couto, Viswanathan, and Moura (2022), the solid-phase volume-averaged lithium concentration, solid-phase surface lithium concentration, and electrolyte-phase concentrations at the battery terminals are estimated using Padé approximation and Kalman decomposition. In this study, closed-loop PDE backstepping observers are proposed to estimate the lithium concentration in the electrolyte phase.

1.4. Contribution

The main contributions of this paper are:

- The lithium concentration in the electrolyte phase within the negative electrode, the separator, and the positive electrode is estimated using PDE observers. To the best of the authors' knowledge, this is the first study to propose a **closed-loop** PDE backstepping observer for this purpose. In Moura et al. (2016), open-loop observers are proposed for electrolyte lithium concentration estimation, whereas in this study, closed-loop observers are designed.
- In Zhang et al. (2022), electrolyte lithium concentrations at the battery terminals are estimated using Padé approximation. In this study, to the best of our knowledge, this is the first time that **modified boundary conditions** are employed to design an observer for the PDEs governing electrolyte lithium concentration without relying on Padé approximation.
- **Reverse sensitivity analysis** is performed on a $LiFePO_4$ cell to identify the most suitable parameter related to electrolyte lithium concentration for determining the terminal boundary values $c_e^{\pm}(t,0^{\pm})$ to be used in observer design. This study employs an analytical derivation approach that is broadly applicable to various battery chemistries and current profiles.
- By employing the estimated electrolyte concentration and inverting the SPMe voltage function, the solid-phase lithium concentration can be estimated, leading to a more accurate SoC estimation compared to Moura et al. (2016).

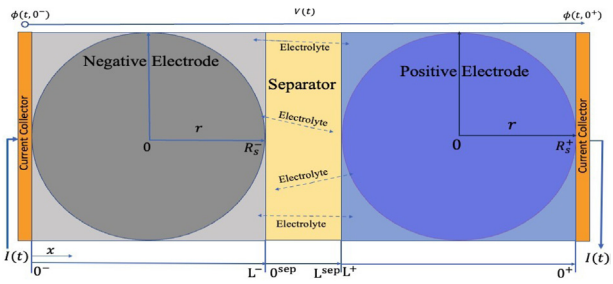

Fig. 1. Schematic of SPMe.

1.5. Organization

The remainder of this paper is organized as follows: In Section 2, the SPMe battery model with modified boundary conditions is described. In Section 3, the availability of electrolyte lithium concentration at the boundaries and reverse sensitivity analysis is explored. Section 4 discusses the proposed electrolyte lithium concentration observers. In Section 5, the solid phase lithium concentration observer and SoC estimation are presented. Observer performance is verified via simulation in Section 6, and Section 7 outlines the conclusion and future work.

2. Battery model

In this section, the SPMe is introduced, followed by a presentation of the modified boundary conditions.

2.1. SPMe

The battery model, SPMe (Moura et al., 2016), schematically illustrated in Fig. 1, is based on the key idea of idealizing the solid phases of each electrode as single spherical particle. t denotes time; r and x represent the radial and spatial coordinates, respectively. Variables and parameters are defined in Table 1. The applied current $I(t)$ and terminal voltage $V(t)$ are the input and output of the system, respectively. The solid-phase lithium concentration $c_s^{\pm}(t,r)$ is governed by:

$$\frac{\partial c_s^{\pm}}{\partial t}(t,r) = \frac{1}{r^2}\frac{\partial}{\partial r}\left[D_s^{\pm} r^2 \frac{\partial c_s^{\pm}}{\partial r}(t,r)\right], \quad t>0, \quad r\in(0,R_s^{\pm}), \tag{1}$$

$$\frac{\partial c_s^{\pm}}{\partial r}(t,0) = 0, \quad t \geq 0, \tag{2}$$

$$\frac{\partial c_s^{\pm}}{\partial r}\left(t,R_s^{\pm}\right) = \pm\frac{1}{D_s^{\pm} F a_s^{\pm} L^{\pm}} I(t), \quad t \geq 0, \tag{3}$$

$$c_s^{\pm}(0,r) = c_{s,0}^{\pm}(r), \quad r\in\left[0,R_s^{\pm}\right], \tag{4}$$

where the specific interfacial area of the electrodes is given by $a_s^{\pm} = \frac{3\varepsilon_s^{\pm}}{R_s^{\pm}}$.

The electrolyte lithium concentration dynamics in the negative electrode, separator, and positive electrode are:

$$\frac{\partial c_e^{\pm}}{\partial t}(t,x) = \frac{D_e^{\pm,\mathrm{eff}}\left(c_e^{\pm}(t,x)\right)}{\varepsilon_e^{\pm}}\frac{\partial^2 c_e^{\pm}(t,x)}{\partial x^2} \mp \frac{(1-t_c^0)}{\varepsilon_e^{\pm} F L^{\pm}} I(t), \tag{5}$$

$$\frac{\partial c_e^{\mathrm{sep}}}{\partial t}(t,x) = \frac{D_e^{\mathrm{sep,eff}}\left(c_e^{\mathrm{sep}}(t,x)\right)}{\varepsilon_e^{\mathrm{sep}}}\frac{\partial^2 c_e^{\mathrm{sep}}(t,x)}{\partial x^2}, \tag{6}$$

where $t>0$ and $x\in(0,L^j), j\in\{-,\mathrm{sep},+\}$ with the following boundary conditions:

$$\frac{\partial c_e^{\pm}}{\partial x}(t,0^{\pm}) = 0, t\geq 0, \tag{7}$$

Table 1
Nomenclature.

Variables	
$c_s^{\pm}$	Solid phase lithium concentration $\left[\text{mol/m}^3\right]$
c_e^j	Electrolyte phase lithium concentration $\left[\text{mol/m}^3\right]$
$j_n^{\pm}$	Molar ion flux $\left[\text{mol/}\left(\text{m}^2\ \text{s}\right)\right]$
$i_0^{\pm}$	Exchange current density $\left[\text{A/m}^2\right]$
I	Applied current $\left[\text{A/m}^2\right]$
V	Terminal voltage [V]
Parameters	
L^j	Length of region [m]
$D_s^{\pm}$	Solid phase diffusion coefficient $\left[\text{m}^2/\text{s}\right]$
D_e^j	Electrolyte phase diffusion coefficient $\left[\text{m}^2/\text{s}\right]$
$\varepsilon_s^{\pm}, \varepsilon_e^j$	Volume fraction: solid, electrolyte phase[–]
t_c^0	Transference number of the ions [–]
F	Faraday's constant [C/mol]
$\sigma^{\pm}, \kappa_e^{\pm}$	Conductivity: solid, electrolyte phase [1/ (Ω m)]
$k^{\pm}$	Kinetic reaction rate $\left[\left(\text{A/m}^2\right)\left(\text{mol}^3/\text{mol}\right)^{(1+\alpha)}\right]$
$R_s^{\pm}$	Particle radius of solid phase [m]
R_f	Solid-electrolyte interphase film resistance $\left[\Omega\ \text{m}^2\right]$
R	Universal gas constant [J/ (mol K)]
$f_{c/a}$	Electrolyte mean molar activity coefficient [–]
brug	Bruggman exponent [–]

$$D_e^{-,\text{eff}}\left(c_e^-(t,x)\right)\frac{\partial c_e^-}{\partial x}(t,L^-) = D_e^{\text{sep,eff}}\left(c_e^{\text{sep}}(t,x)\right)\frac{\partial c_e^{\text{sep}}(t,0^{\text{sep}})}{\partial x},\ t\geq 0, \tag{8}$$

$$D_e^{+,\text{eff}}\left(c_e^+(t,x)\right)\frac{\partial c_e^+}{\partial x}(t,L^+) = D_e^{\text{sep,eff}}\left(c_e^{\text{sep}}(t,x)\right)\frac{\partial c_e^{\text{sep}}(t,L^{\text{sep}})}{\partial x},\ t\geq 0, \tag{9}$$

$$c_e^-\left(t,L^-\right) = c_e^{\text{sep}}\left(t,0^{\text{sep}}\right),\ t\geq 0, \tag{10}$$

$$c_e^{\text{sep}}\left(t,L^{\text{sep}}\right) = c_e^+\left(t,L^+\right),\ t\geq 0, \tag{11}$$

$$c_e^j(0,x) = c_{e,0}^j(x), x\in\left[0,L^j\right], j\in\{-,\text{sep},+\}. \tag{12}$$

The terminal voltage $V(t)$ of the battery model is:

$$\begin{aligned}V(t) &= \frac{\text{RT}}{\alpha F}\sinh^{-1}\left(\frac{-I(t)}{2a_s^+L^+\bar{i}_0^+(t)}\right)\\ &- \frac{\text{RT}}{\alpha F}\sinh^{-1}\left(\frac{I(t)}{2a_s^-L^-\bar{i}_0^-(t)}\right)\\ &+ U^+\left(c_{ss}^+(t)\right) - U^-\left(c_{ss}^-(t)\right)\\ &- \left(\frac{R_f^+}{a_s^+L^+} + \frac{R_f^-}{a_s^-L^-} - \frac{L^+ + 2L^{\text{sep}} + L^-}{2\kappa_e}\right)I(t)\\ &+ k_{\text{conc}}(t)\left[\ln c_e^+\left(t,0^+\right) - \ln c_e^-\left(t,0^-\right)\right]\\ &\triangleq \nu_1\left(t,I(t),c_{ss}^{\pm}(t),c_e^{\pm}(t,0^{\pm})\right),\end{aligned} \tag{13}$$

where $c_{ss}^{\pm}(t)\triangleq c_s^{\pm}(t,R_s^{\pm})$. The function $\nu_1(\cdot)$ captures the detailed dependencies of the SPMe voltage function. Averaged exchange current density is given by:

$$\bar{i}_0^{\pm}(t) = k^{\pm}\left[c_{ss}^{\pm}(t)\right]^{\frac{1}{2}}\left[c_{e,0}^{\pm}\left(c_{s,\max}^{\pm} - c_{ss}^{\pm}(t)\right)\right]^{\frac{1}{2}}, \tag{14}$$

and $k_{\text{conc}}(t) = \frac{2RT(1-t_c^0)}{F}\left(1+\frac{d\ln f_{c/a}(t,0^{\pm})}{d\ln c_e^{\pm}(t,0^{\pm})}\right)$. The term $\frac{d\ln f_{c/a}(t,0^{\pm})}{d\ln c_e^{\pm}(t,0^{\pm})}$ is relative logarithmic derivative, representing normalized sensitivity of $f_{c/a}(t,0^{\pm})$ to $c_e^{\pm}(t,0^{\pm})$.

2.2. Modified boundary conditions

The coupled boundary conditions in the electrolyte concentration PDEs (8) and (9) complicate observer design. To address this, modified uncoupled boundary conditions are employed under the following assumptions.

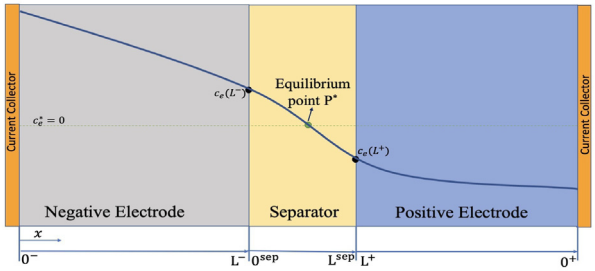

Fig. 2. Electrolyte-phase modified boundary condition.

Assumption 1. Total moles of lithium in the electrolyte phase $n_{\text{Li,e}}$ is conserved.

An equilibrium point P^* is defined as the location in the separator where the lithium ion flux is balanced between the left and right sides. Under Assumption 1, the total flux entering from the negative electrode and the separator region up to P^* is assumed to equal the total flux exiting through the remaining separator region and the positive electrode.

Assumption 2. The solid-phase current density $i_s^{\pm}(t,x)$ and the electrolyte current density $i_e^{\pm}(t,x)$ are approximated by their respective average values $\bar{i}_s^{\pm}(t)$ and $\bar{i}_e^{\pm}(t)$.

Using Assumptions 1 and 2, the conservation of electrolyte lithium ions at P^* is characterized as follows (Xu, Wang, Pei, Mao, & Zhu, 2020):

$$\begin{aligned}&\frac{\bar{i}_e^-(t)+\bar{i}_s^-(t)}{F}L^- + \frac{\bar{i}_e^{\text{sep}}(t)}{F}P^*\\ &= \frac{\bar{i}_e^{\text{sep}}(t)}{F}(L^{\text{sep}}-P^*) + \frac{\bar{i}_e^+(t)+\bar{i}_s^+(t)}{F}L^+.\end{aligned} \tag{15}$$

Total current density in the electrodes and separator are:

$$\bar{i}_e^{\pm}(t) + \bar{i}_s^{\pm}(t) = \bar{i}_e^{\text{sep}}(t) = \frac{I(t)}{A}. \tag{16}$$

Substituting (16) into (15) yields the position of P^* (Sepasiahooyi & Tang, 2024a):

$$P^* = \frac{L^+ + L^{\text{sep}} - L^-}{2}. \tag{17}$$

The quasi-linear behavior of lithium concentration within the separator domain is assumed, meaning that the concentration is approximated to vary linearly with respect to position, as shown in Fig. 2. Although the actual profile may exhibit some nonlinearities, this assumption is sufficiently accurate for observer design. This assumption, combined with the condition $c_e^{\text{sep}}(t,P^*) = 0$, leads to the following linear gradient-based boundary conditions:

$$\frac{\partial c_e^-}{\partial x}(t,L^-) = \frac{-c_e^-(t,L^-)}{P^*}, \tag{18}$$

$$\frac{\partial c_e^+}{\partial x}(t,L^+) = \frac{c_e^+(t,L^+)}{L^{\text{sep}}-P^*}. \tag{19}$$

Note that the boundary conditions (10) and (11) remain unchanged. As a result, the electrolyte lithium concentration dynamics in the negative electrode, separator, and the positive electrode, with the boundary conditions at the terminal boundaries (7), coupled boundary conditions (10) and (11), and the modified uncoupled boundary conditions (18) and (19), form a cascaded system.

3. Availability of electrolyte lithium concentration at the boundaries $c_e^{\pm}(t, 0^{\pm})$

For the closed-loop electrolyte observer, it is essential to determine $c_e^{\pm}(t, 0^{\pm})$, which can be estimated using its relationship with other measurable parameters, such as the electrolyte diffusion coefficient $D_e^{\pm}(t, 0^{\pm})$ at the boundaries (Newman & Balsara, 2021, Eq. (12.12)):

$$D_e^{\pm}\left(c_e^{\pm}(t,0^{\pm})\right) = \mathscr{D}\frac{c_e^{\pm}(t,0^{\pm})}{c_{\text{solv}}} \times \left(1 + \frac{d\ln \bar{\gamma}^{\pm}\left(\mathcal{I}_{\text{ion}}(m(t))\right)}{d\ln m(t)}\right), \tag{20}$$

where $\mathscr{D}$ is the diffusion coefficient for the interaction of species, and its value has been determined using the nuclear magnetic resonance technique (Karatrantos et al., 2021) and c_{solv} is the reference concentration of the solvent. In Newman and Balsara (2021), the mean molal activity coefficient $\bar{\gamma}^{\pm}$ is assumed to be constant. In this study, to improve accuracy, $\bar{\gamma}^{\pm}\left(\mathcal{I}_{\text{ion}}(m(t))\right)$ is treated as a function of the ionic strength $\mathcal{I}_{\text{ion}}(m(t))$, where $m(t)$ is the electrolyte molality. The term $\frac{d\ln \bar{\gamma}^{\pm}(\mathcal{I}_{\text{ion}}(m(t)))}{d\ln m(t)}$ represents the relative logarithmic derivative, which provides a dimensionless normalized sensitivity. The molal activity coefficients of the electrolyte salt species $\gamma_i(\mathcal{I}_{\text{ion}}(m(t)))$, $i \in \{\text{an}, \text{ca}\}$ (i.e., anion and cation), in moderately concentrated electrolytes are described by the Davies equation (Cerrillo-Gonzalez, Villen-Guzman, Vereda-Alonso, Rodríguez-Maroto, & Paz-Garcia, 2022, Eq. (12.12)):

$$\log \gamma_i\left(\mathcal{I}_{\text{ion}}\left(m(t)\right)\right) = -\mathcal{A}_{\text{Dav}} z_i^2 \times \left(\frac{\sqrt{\mathcal{I}_{\text{ion}}\left(m(t)\right)}}{1+\sqrt{\mathcal{I}_{\text{ion}}\left(m(t)\right)}} - 0.3\mathcal{I}_{\text{ion}}\left(m(t)\right)\right), \tag{21}$$

for $i \in \{\text{an}, \text{ca}\}$. Here, $\mathcal{A}_{\text{Dav}} = 0.5085$ and z_i, $i \in \{\text{an}, \text{ca}\}$ is the ionic charge of the electrolyte salt species, with $z_{\text{ca}} = +1$ and $z_{\text{an}} = -1$. The molal ionic strength is defined as Newman and Balsara (2021, Eq. (4.26)):

$$\mathcal{I}_{\text{ion}}\left(m(t)\right) = \frac{1}{2}\sum_{i\in\{\text{an},\text{ca}\}} z_i^2 m_i(t). \tag{22}$$

Given that most electrolyte salts in lithium-ion batteries are of the type 1:1 (e.g., $LiPF_6$), the resulting cation and anion molalities are equal, i.e., $m_{\text{ca}}(t) = m_{\text{an}}(t)$. Under the full dissociation assumption, all dissolved salt dissociates completely into its ionic constituents, and each of these ion molalities becomes equal to the total salt molality, i.e., $m_{\text{ca}}(t) = m_{\text{an}}(t) = m(t)$. Consequently, Eq. (22) simplifies to:

$$\mathcal{I}_{\text{ion}}\left(m(t)\right) = m(t). \tag{23}$$

Substitution of (23) into (21) yields:

$$\ln \gamma_i\left(m(t)\right) = -A_{\text{Dav}}\ln(10) z_i^2\left(\frac{\sqrt{m(t)}}{1+\sqrt{m(t)}} - 0.3\, m(t)\right). \tag{24}$$

For simplicity, it is assumed that $\gamma_{\text{ca}}(m(t)) \approx \gamma_{\text{an}}(m(t)) \approx \bar{\gamma}^{\pm}(m(t))$. Therefore, the last term in (20), obtained by differentiating (24) with respect to $m(t)$, is derived as:

$$\frac{d\ln \bar{\gamma}^{\pm}\left(m(t)\right)}{d\ln m(t)} = \frac{d\ln \bar{\gamma}^{\pm}\left(m(t)\right)}{dm(t)}\cdot\frac{dm(t)}{d\ln m(t)} = \frac{d\ln \bar{\gamma}^{\pm}\left(m(t)\right)}{dm(t)} m(t) = \mathcal{A}_{\text{Dav}}\ln(10)(z^{\pm})^2 \times m(t)\left(\frac{-1}{2\sqrt{m(t)}(1+\sqrt{m(t)})^2} + 0.3\right), \tag{25}$$

where $z^{\pm}$ denotes the ionic charge magnitude for either cation or anion. Although the electrolyte molality $m(t)$ typically represents a bulk property, for consistency with the boundary concentration, a pointwise molality $m^{\pm}(t)$ is defined by adapting the expression in Newman and Balsara (2021, Eq. (2.17)) as follows:

$$m^{\pm}(t) = \frac{c_e^{\pm}(t,0^{\pm})}{\rho - M c_e^{\pm}(t,0^{\pm})}, \tag{26}$$

where ρ and M are the density of the solution and the molar mass of the electrolyte salt, respectively.

The reverse sensitivity of $c_e^{\pm}(t, 0^{\pm})$ to $D_e^{\pm}(c_e^{\pm}(t, 0^{\pm}))$ is:

$$\frac{\partial D_e^{\pm}\left(c_e^{\pm}(t,0^{\pm})\right)}{\partial c_e^{\pm}(t,0^{\pm})} = \frac{\mathscr{D}}{c_{\text{solv}}}\left(1 + \frac{d\ln \bar{\gamma}^{\pm}\left(m^{\pm}(t)\right)}{d\ln m^{\pm}(t)}\right) + \frac{\mathscr{D}c_e^{\pm}(t,0^{\pm})}{c_{\text{solv}}}\left(\mathcal{A}_{\text{Dav}}\ln(10)z^2\frac{\left(1-m^{\pm}(t)\right)}{4\sqrt{m^{\pm}(t)}\left(1+m^{\pm}(t)\right)^3} + 0.3\ln(10)z^2\left(\frac{\rho}{\left(\rho - M c_e^{\pm}(t,0^{\pm})\right)^2}\right)\right) \triangleq h(t). \tag{27}$$

Remark 1. $D_e^{\pm}(t, 0^{\pm})$ can also be expressed as an exponential function of electrolyte concentration, based on molecular dynamics simulations (Ravikumar, Mynam, & Rai, 2018):

$$D_e^{\pm}(c_e^{\pm}(t,0^{\pm})) = D_0\exp\left(-\frac{c_e^{\pm}(t,0^{\pm})}{C_D}\right), \tag{28}$$

where D_0 is the diffusion coefficient at infinite dilution, available in Ravikumar et al. (2018) for a $LiFePO_4$ cell. C_D is the Arrhenius fitting constant, set to 0.472.

Another measurement related to $c_e^{\pm}(t, x)$ is the electrolyte conductivity $\kappa_e^{\pm}(c_e^{\pm}(t, x))$, given by the Einstein relation (Ecker et al., 2015):

$$\kappa_e^{\pm}(c_e^{\pm}(t,x)) = \frac{e^2 N_A D_e^{\pm}(c_e^{\pm}(t,x))\, c_e^{\pm}(t,x)}{k_B T}, \tag{29}$$

where T denotes the temperature, assumed constant throughout this study. k_B, e, and N_A denote the Boltzmann constant, the elementary charge, and the Avogadro constant, respectively. Due to the dependency of $\kappa_e^{\pm}(c_e^{\pm}(t, 0^{\pm}))$ not only on $c_e^{\pm}(t, 0^{\pm})$ but also on $D_e^{\pm}(c_e^{\pm}(t, 0^{\pm}))$, conducting forward sensitivity analysis is complex; therefore, a reverse sensitivity analysis is performed. Using (27) and (29), reverse sensitivity of $c_e^{\pm}(t, 0^{\pm})$ to $\kappa_e^{\pm}(c_e^{\pm}(t, 0^{\pm}))$ is derived as: $\frac{\partial \kappa_e^{\pm}(c_e^{\pm}(t,0^{\pm}))}{\partial c_e^{\pm}(t,0^{\pm})} = \frac{e^2 N_A}{k_B T}\left(D_e^{\pm}(c_e^{\pm}(t,0^{\pm})) + c_e^{\pm}(t,0^{\pm})\, h(t)\right)$.

Furthermore, the electrolyte resistance $R_e^{\pm}(c_e^{\pm}(t, 0^{\pm}))$ is another parameter related to $c_e^{\pm}(t, 0^{\pm})$ as follows (Sepasiahooyi & Tang, 2024c):

$$R_e^{\pm}(c_e^{\pm}(t,0^{\pm})) = \frac{L^{\pm}}{2A\kappa_e^{\pm,\text{eff}}\left(c_e^{\pm}(t,0^{\pm})\right)}, \tag{30}$$

where $\kappa_e^{\pm,\text{eff}}\left(c_e^{\pm}(t,0^{\pm})\right) = \kappa_e^{\pm}\left(c_e^{\pm}(t,0^{\pm})\right)\cdot\left(\varepsilon_e^{\pm}\right)^{\text{brug}}$ is the effective electrolyte conductivity. The reverse sensitivity of $c_e^{\pm}(t, 0^{\pm})$ to $R_e^{\pm}(c_e^{\pm}(t, 0^{\pm}))$ is:

$$\frac{\partial R_e^{\pm}(c_e^{\pm}(t,0^{\pm}))}{\partial c_e^{\pm}(t,0^{\pm})} = -\frac{L^{\pm}}{2A\left(\kappa_e^{\pm,\text{eff}}(c_e^{\pm}(t,0^{\pm}))\right)^2} \times \frac{e^2 N_A}{k_B T}\left(D_e^{\pm}(c_e^{\pm}(t,0^{\pm})) + c_e^{\pm}(t,0^{\pm})h(t)\right). \tag{31}$$

Remark 2. Measuring parameters at the terminal boundaries requires localized Electrochemical Impedance Spectroscopy (EIS), which is an offline technique. Typically, acquiring an EIS spectrum, which involves measurements at 60 frequencies spanning

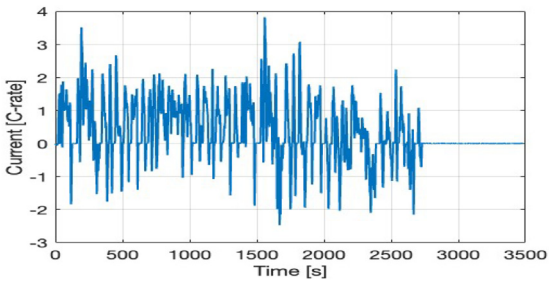

Fig. 3. UDDS current profile.

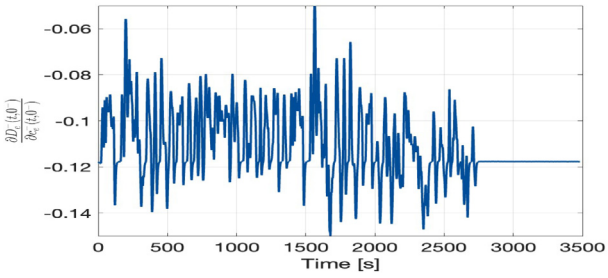

Fig. 4. Reveres sensitivity of $c_e^-(t,0^-)$ to $D_e^-(c_e^-(t,0^-))$.

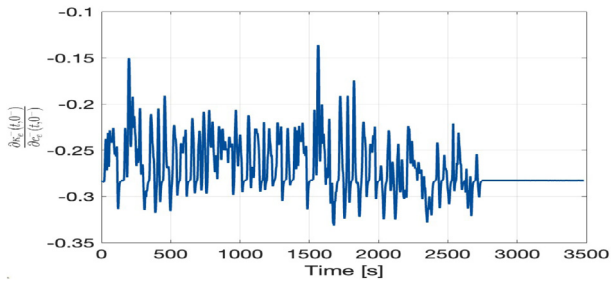

Fig. 5. Reveres sensitivity of $c_e^-(t,0^-)$ to $\kappa_e^-(c_e^-(t,0^-))$.

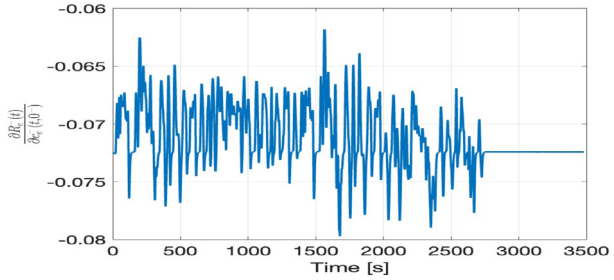

Fig. 6. Reveres sensitivity of $c_e^-(t,0^-)$ to $R_e^-(c_e^-(t,0^-))$.

from 100 kHz to 0.1 Hz, requires approximately 2 to 3 min to accomplish (Lazanas & Prodromidis, 2023). Integrating event-triggered mechanisms into the observer is a future work to address the offline nature of EIS.

This analysis is applied to an $LiFePO_4$ cell, using the specifications provided in Chiew, Chin, Toh, Gao, and Zhang (2019), under the Urban Dynamometer Driving Schedule (UDDS) current profile shown in Fig. 3, and assuming a constant temperature of $T = 298$ K. The density of the solution and the molar mass are taken to be $\rho = 1289$ kg/m^3 and $M = 0.151$ kg/mol, respectively. To reflect EIS measurement noise, zero-mean Gaussian noise with a standard deviation of 2% (Lazanas & Prodromidis, 2023) is added to the measurements. The reverse sensitivities of $c_e^-(t,0^-)$ to $D_e^-(c_e^-(t,0^-))$, $\kappa_e^-(c_e^-(t,0^-))$, and $R_e^-(c_e^-(t,0^-))$ are illustrated in Fig. 4, Fig. 5, and Fig. 6, respectively. Due to space constraints, the simulation plots for the positive electrode are omitted and can be found in Sepasiahooyi and Tang (2024b). A comparison of the results reveals that, for $LiFePO_4$ cells, the electrolyte resistance at the boundaries exhibits the least variation with respect to changes in electrolyte concentration. The reverse sensitivity analysis indicates that $c_e^-(t,0^-)$ is more sensitive to $R_e^-(t,0^-)$, suggesting that $R_e^-(t,0^-)$ is the most reliable boundary measurement for obtaining $c_e^-(t,0^-)$ to employ in the observer design. Although the sensitivity simulation results may vary depending on parameters and battery chemistries, the proposed approach is generic and applicable to a variety of batteries and different current profiles.

4. Electrolyte lithium concentration observers

In this section, backstepping PDE observers are designed for the electrolyte phase, beginning with the negative electrode, followed by the separator, and then the positive electrode. For observer design purpose, we simplify the model (5)–(12) and make the following assumption:

Assumption 3. The effective electrolyte diffusion coefficient $D_e^{j,\text{eff}}(c_e^j(t,x)) = D_e^j\left(c_e^j(t,x)\right)\cdot\left(\varepsilon_e^j\right)^{\text{brug}}$, $j \in \{-,\text{sep},+\}$, is considered constant.

To facilitate observer design, the electrolyte PDEs are first normalized using the following coordinate changes:

$$\bar{x} = \frac{x}{L^j},\ \bar{t} = \frac{D_e^{j,\text{eff}}}{(L^j)^2\varepsilon_e^j}t, \tag{32}$$

where $j \in \{-,\text{sep},+\}$. The negative electrode concentration dynamic, (5), (7), and (18), is normalized as:

$$\frac{\partial c_e^-}{\partial \bar{t}}(\bar{t},\bar{x}) = \frac{\partial^2 c_e^-}{\partial \bar{x}^2}(\bar{t},\bar{x}) + \frac{L^-(1-t_c^0)}{D_e^{-,\text{eff}}F}I(\bar{t}), \tag{33}$$

$$\frac{\partial c_e^-}{\partial \bar{x}}(\bar{t},0^-) = 0, \tag{34}$$

$$\frac{\partial c_e^-}{\partial \bar{x}}(\bar{t},1^-) = \frac{-L^- c_e^-(\bar{t},1^-)}{P^*}. \tag{35}$$

A backstepping closed-loop observer for the normalized electrolyte lithium concentration PDEs in the negative electrode (33)–(35) is designed as follows:

$$\frac{\partial \hat{c}_e^-}{\partial \bar{t}}(\bar{t},\bar{x}) = \frac{\partial^2 \hat{c}_e^-}{\partial \bar{x}^2}(\bar{t},\bar{x}) + \frac{L^-(1-t_c^0)}{D_e^{-,\text{eff}}F}I(\bar{t}) + \bar{k}_1^-(\bar{x})(c_e^-(\bar{t},0^-) - \hat{c}_e^-(\bar{t},0^-)), \tag{36}$$

$$\frac{\partial \hat{c}_e^-}{\partial \bar{x}}(\bar{t},0^-) = \bar{k}_{10}^-(c_e^-(\bar{t},0^-) - \hat{c}_e^-(\bar{t},0^-)), \tag{37}$$

$$\frac{\partial \hat{c}_e^-}{\partial \bar{x}}(\bar{t},1^-) = \frac{-L^-\hat{c}_e^-(\bar{t},1^-)}{P^*}, \tag{38}$$

where $\bar{k}_1^-(\bar{x})$ and $\bar{k}_{10}^-$ are observer gains, tuned to guarantee the stability of the state estimation error system $\tilde{c}_e^-(\bar{t},\bar{x}) = c_e^-(\bar{t},\bar{x}) - \hat{c}_e^-(\bar{t},\bar{x})$.

$$\frac{\partial \tilde{c}_e^-}{\partial \bar{t}}(\bar{t},\bar{x}) = \frac{\partial^2 \tilde{c}_e^-}{\partial \bar{x}^2}(\bar{t},\bar{x}) - \bar{k}_1^-(\bar{x})\tilde{c}_e^-(\bar{t},0^-), \tag{39}$$

$$\frac{\partial \tilde{c}_e^-}{\partial \bar{x}}(\bar{t},0^-) = -\bar{k}_{10}^-\tilde{c}_e^-(\bar{t},0^-), \tag{40}$$

$$\frac{\partial \tilde{c}_e^-}{\partial \bar{x}}(\bar{t},1^-) = \frac{-L^-\tilde{c}_e^+(\bar{t},1^-)}{P^*}. \tag{41}$$

We aim to determine an invertible transformation:

$$\tilde{c}_e^-(\bar{t},\bar{x}) = \tilde{w}(\bar{t},\bar{x}) - \int_0^{\bar{x}} \bar{k}(\bar{x},y)\tilde{w}(\bar{t},y)dy, \tag{42}$$

which satisfies the exponentially stable target system:

$$\frac{\partial \tilde{w}}{\partial \bar{t}}(\bar{t},\bar{x}) = \frac{\partial^2 \tilde{w}}{\partial \bar{x}^2}(\bar{t},\bar{x}) - \alpha\tilde{w}(\bar{t},\bar{x}), \tag{43}$$

$$\frac{\partial \tilde{w}}{\partial \bar{x}}(\bar{t},0^-) = 0, \tag{44}$$

$$\frac{\partial \tilde{w}}{\partial \bar{x}}(\bar{t},1^-) = -q^-\tilde{w}(\bar{t},1^-), \tag{45}$$

where $q^- = \frac{L^-}{P^*}$, and $\alpha > \frac{1}{4}$ is a parameter that determines the convergence rate. From (39)–(45), the kernel system is obtained:

$$\frac{\partial^2 \bar{k}}{\partial \bar{x}^2}(\bar{x},y) - \frac{\partial^2 \bar{k}}{\partial y^2}(\bar{x},y) = -\alpha\bar{k}(\bar{x},y), \tag{46}$$

$$\frac{\partial \bar{k}}{\partial \bar{x}}(1,y) = -q^-\bar{k}(1,y), \tag{47}$$

$$\bar{k}(\bar{x},\bar{x}) = -\frac{\alpha}{2}\bar{x}. \tag{48}$$

Solution of the kernel function is achieved as follows (Rathnayake, Diagne, Espitia, & Karafyllis, 2021):

$$\begin{aligned}\bar{k}(\bar{x},y) &= \frac{-\alpha q^-}{\sqrt{\alpha+(q^-)^2}} \\ &\times \int_0^{\bar{x}-y} e^{q^-\tau/2} I_0\left(\sqrt{\alpha(2-\bar{x}-y)(\bar{x}-y-\tau)}\right) \\ &\times \sinh\left(\frac{\sqrt{\alpha+(q^-)^2}}{2}\tau\right) d\tau \\ &- \alpha(1-y)\frac{I_1\left(\sqrt{\alpha\left((1-y)^2-(1-\bar{x})^2\right)}\right)}{\sqrt{\alpha\left((1-y)^2-(1-\bar{x})^2\right)}},\end{aligned} \tag{49}$$

where $I_m(\cdot)$, $m \in \{0,1\}$, denotes the modified Bessel functions of the first kind of zero and first order (Krstic & Smyshlyaev, 2008). Accordingly, the observer gains $\bar{k}_1^-(\bar{x})$ and $\bar{k}_{10}^-$ will be obtained as:

$$\bar{k}_1^-(\bar{x}) = \alpha\bar{k}_y(\bar{x},0), \tag{50}$$

$$\bar{k}_{10}^- = -\frac{\alpha}{2}. \tag{51}$$

Lemma 1. *Consider the normalized electrolyte lithium concentration PDE in the negative electrode (33)–(35) and the proposed state observer (36)–(38). For any initial data $\hat{c}_e^-(0,\cdot) \in L^2(0,1)$, under Assumptions 3–2, if $\alpha > \frac{1}{4}$, then by selecting the observer gains in (50) and (51), the estimation error system (39)–(41) is exponentially stable in the sense of the L^2 norm, in the presence of boundary measurement error. This implies that states of the observer (36)–(38) converge exponentially to the states of the system (33)–(35) in the spatial L^2 norm.*

Proof. The detailed proof with the Lyapunov function $V_1(\bar{t}) = \frac{1}{2}\int_0^{1^-} \tilde{\omega}^2(\bar{t},\bar{x})d\bar{x}$ is provided in Baccoli, Orlov, and Pisano (2014). □

The observer for the electrolyte lithium concentration within the negative electrode in the original unnormalized system (5), (7), and (18) is derived as follows:

$$\begin{aligned}\frac{\partial \hat{c}_e^-}{\partial t}(t,x) &= \frac{D_e^{-,\text{eff}}}{\varepsilon_e^-}\frac{\partial^2 \hat{c}_e^-}{\partial x^2}(t,x) + \frac{1-t_c^0}{FL^-\varepsilon_e^-}I(t) \\ &+ k_1^-(x)\tilde{c}_e^-(t,0^-),\end{aligned} \tag{52}$$

$$\frac{\partial \hat{c}_e^-}{\partial x}(t,0^-) = k_{10}^-\tilde{c}_e^-(t,0^-), \tag{53}$$

$$\frac{\partial \hat{c}_e^-}{\partial x}(t,L^-) = \frac{\hat{c}_e^-(t,L^-)}{P^*}, \tag{54}$$

where the observer gains are:

$$k_1^-(x) = \frac{D_e^{-,\text{eff}}}{(L^-)^2\varepsilon_e^-}\bar{k}_1^-(x), \tag{55}$$

$$k_{10}^- = \frac{\bar{k}_{10}^-}{L^-}. \tag{56}$$

Lemma 2. *Consider the electrolyte lithium concentration PDE in the negative electrode (5), (7), and (18), and the state observer (52)–(54). For any initial data $\hat{c}_e^-(0,\cdot) \in L^2(0^-,L^-)$, under Assumptions 3–2, if $\alpha > \frac{1}{4}$, by selecting the observer gains as defined in (55) and (56), the states of the observer converge exponentially to the states of the original system in the spatial L^2 norm.*

Proof. Due to the coordinate changes (32), the stability of the observer for the original system in Lemma 2 directly follows Lemma 1. □

The electrolyte lithium concentration observer in the separator operates in cascade with the electrolyte observer in the negative electrode, using the estimated boundary value $\hat{c}_e^-(t,L^-)$ obtained from the negative side to generate the boundary error for separator observer. The separator observer is first designed for the normalized system, similarly to the negative electrode. Then, the observer for electrolyte lithium concentration within the separator in the original system (6), (10), (11), (18) and (19) is proposed as:

$$\begin{aligned}\frac{\partial \hat{c}_e^{\text{sep}}}{\partial t}(t,x) &= \frac{D_e^{\text{sep,eff}}}{\varepsilon_e^{\text{sep}}}\frac{\partial^2 \hat{c}_e^{\text{sep}}}{\partial x^2}(t,x) \\ &+ k_1^{\text{sep}}(x)(\hat{c}_e^-(t,L^-) - \hat{c}_e^{\text{sep}}(t,0^{\text{sep}})),\end{aligned} \tag{57}$$

$$\begin{aligned}\frac{\partial \hat{c}_e^{\text{sep}}}{\partial x}(t,0^{\text{sep}}) &= \frac{\hat{c}_e^-(t,0^{\text{sep}})}{P^*} \\ &- k_{10}^{\text{sep}}(\hat{c}_e^-(t,L^-) - \hat{c}_e^{\text{sep}}(t,0^{\text{sep}})),\end{aligned} \tag{58}$$

$$\frac{\partial \hat{c}_e^{\text{sep}}}{\partial x}(t,L^{\text{sep}}) = \frac{\hat{c}_e^+(t,L^{\text{sep}})}{P^*+L^--L^+}, \tag{59}$$

where observer gains are defined as follows:

$$k_1^{\text{sep}}(x) = \frac{\alpha D_e^{\text{sep,eff}}}{(L^{\text{sep}})^2\varepsilon_e^{\text{sep}}}\bar{k}_y(x,0), \tag{60}$$

$$k_{10}^{\text{sep}} = -\frac{\alpha}{2L^{\text{sep}}} - \frac{1}{P^*L^{\text{sep}}}. \tag{61}$$

Lemma 3. *Consider the electrolyte lithium concentration PDE in the separator (6), (10), (11), (18), and (19), and the proposed state observer (57)–(59). For any initial data $\hat{c}_e^{sep}(0,\cdot) \in L^2(0^{sep},L^{sep})$, under Assumptions 3–2, and for any $\alpha > \frac{1}{4}$, if the observer gains are chosen as in (60) and (61), the observer states converge exponentially to the true separator states in the spatial L^2 norm.*

Proof. The convergence of the proposed separator observer (57)–(59) can be proved similar to Lemma 2, based on a similar coordinate changes as in (32) and Lyapunov function for the normalized system: $V_2(\bar{t}) = \frac{1}{2}\int_0^{1^{\text{sep}}} \tilde{\omega}^2(\bar{t},\bar{x})d\bar{x}$. □

Theorem 1. *The separator observer (57)–(59) operates in **cascade** with the electrolyte observer in the negative electrode (52)–(54),*

where the estimated boundary value $\hat{c}_e^-(t, L^-)$, obtained from the negative electrode observer, is used to drive the separator observer. Given that the negative electrode and separator observers are exponentially stable (as shown in Lemmas 2 and 3, respectively), the overall cascaded observer system for any initial data $\hat{c}_e^-(0,\cdot) \in L^2(0^-, L^-)$ and $\hat{c}_e^{sep}(0,\cdot) \in L^2(0^{sep}, L^{sep})$, under Assumptions 3–2, and for any $\alpha > \frac{1}{4}$ is exponentially stable in the L^2 norm.

Proof. The convergence of the cascaded $(\hat{c}_e^-, \hat{c}_e^{sep})$-observer follows directly. A rigorous proof can be conducted in two steps. First, the convergence of the normalized cascaded observer can be established using the weighted Lyapunov function $V_3(t) = aV_1(t) + V_2(t)$, with $a > 0$ being an appropriately chosen positive weighting constant. Then, the convergence of the original cascaded $(\hat{c}_e^-, \hat{c}_e^{sep})$ observer follows by applying the corresponding coordinate changes (32). □

For electrolyte observer in the positive electrode, instead of using the estimated boundary value from the separator observer, we utilize EIS measurements to obtain $c_e^+(t, 0^+)$. The observer is first designed for the normalized system, following the negative electrode procedure. Then observer for the original system is designed as:

$$\frac{\partial \hat{c}_e^+}{\partial t}(t,x) = \frac{D_e^{+,\text{eff}}}{\varepsilon_e^+}\frac{\partial^2 \hat{c}_e^+}{\partial x^2}(t,x) + \frac{1-t_c^0}{FL^+\varepsilon_e^+}I(t) + k_1^+(x)(c_e^+(t,0^+) - \hat{c}_e^+(t,0^+)), \tag{62}$$

$$\frac{\partial \hat{c}_e^+}{\partial x}(t,0^+) = k_{10}^+(c_e^+(t,0^+) - \hat{c}_e^+(t,0^+)), \tag{63}$$

$$\frac{\partial \hat{c}_e^+}{\partial x}(t,L^+) = \frac{\hat{c}_e^+(t,L^+)}{P^* + L^- - L^+}. \tag{64}$$

The observer gains are defined as follows:

$$k_1^+(x) = \frac{\alpha D_e^{+,\text{eff}}}{(L^+)^2\,\varepsilon_e^+}\bar{k}_y(x,0), \tag{65}$$

$$k_{10}^+ = -\frac{\alpha}{2L^+}. \tag{66}$$

Here, q^- in (49) is replaced by $q^+ = \frac{-L^+}{P^*+L^--L^+}$.

Theorem 2. *Consider the electrolyte lithium concentration PDE in the positive electrode (5), (7), and (19), along with the proposed state observer (62)–(64). For any initial data $\hat{c}_e^+(0,\cdot) \in L^2(L^+, 0^+)$, under Assumptions 3–2, if $\alpha > \frac{1}{4}$, then by selecting the observer gains as in (65) and (66), with q^- replaced by $q^+ = \frac{-L^+}{P^*+L^--L^+}$, the states of the designed observer converge exponentially to the states of the original system in the spatial L^2 norm.*

Proof. The convergence can be proved similarly to Lemma 2. □

5. Enhanced solid-phase lithium concentration observer

This section first outlines the process of obtaining surface solid-phase lithium concentration in the positive electrode $c_{ss}^+(t)$. Subsequently, the solid-phase observers and SoC estimation are presented.

5.1. Availability of $c_{ss}^+(t)$ via voltage function inversion

To obtain $c_{ss}^+(t)$, the battery voltage $V(t)$ (13) is used. Given that $V(t)$ and $c_e^\pm(t, 0^\pm)$ are measurable, a relationship between $c_{ss}^+(t)$ and $c_{ss}^-(t)$, if available, allows $c_{ss}^+(t)$ to be obtained via inversion of the voltage function. The total moles of lithium in the solid phase are given by (Moura et al., 2014):

$$n_{\text{Li},s}(t) = \sum_{i\in\{+,-\}} \frac{\varepsilon_s^i L^i}{\frac{4}{3}\pi\left(R_s^i\right)^3}\int_0^{R_s^i} 4\pi r^2 c_s^i(t,r)dr. \tag{67}$$

Assumption 4. The total number of lithium moles in the solid phase remains constant, i.e., $n_{\text{Li},s}(t) = n_{\text{Li},s}$.

By defining the averaged concentrations as:

$$\bar{c}_s^\pm(t) = \frac{3}{\left(R_s^\pm\right)^3}\int_0^{R_s^\pm} r^2 c_s^\pm(t,r)\,\mathrm{d}r, \tag{68}$$

Eq. (67) can be expressed as:

$$n_{\text{Li},s} = \varepsilon_s^+ L^+ \bar{c}_s^+(t) + \varepsilon_s^- L^- \bar{c}_s^-(t), \tag{69}$$

which gives

$$\bar{c}_s^-(t) = \theta \bar{c}_s^+(t) + \beta, \tag{70}$$

where $\theta = -\frac{\varepsilon_s^+ L^+}{\varepsilon_s^- L^-}$ and $\beta = \frac{n_{\text{Li},s}}{\varepsilon_s^- L^-}$. Moreover, the solid phase lithium concentration dynamics can be approximated using polynomial solution profiles as (Tang et al., 2017):

$$\bar{c}_s^\pm(t) = c_{ss}^\pm(t) - \frac{8R_s^\pm}{35}\bar{q}_s^\pm(t) + \frac{R_s^\pm}{35D_s^\pm}j^\pm(t), \tag{71}$$

where $j^\pm(t) = \mp\frac{I(t)}{a_s^\pm FL^\pm}$ and the volume averaged fluxes $\bar{q}_s^\pm(t)$ satisfy

$$\frac{\mathrm{d}}{\mathrm{d}t}\bar{q}_s^\pm(t) = -\frac{30D_s^\pm}{\left(R_s^\pm\right)^2}\bar{q}_s^\pm(t) - \frac{45}{2\left(R_s^\pm\right)^2}j^\pm(t).$$

Substituting (71) into (70), one obtains:

$$c_{ss}^-(t) = \theta\left(c_{ss}^+(t) - \frac{8R_s^+}{35}\bar{q}_s^+(t) + \frac{R_s^+}{35D_s^+}j^+(t)\right) + \beta + \frac{8R_s^-}{35}\bar{q}_s^-(t) - \frac{R_s^-}{35D_s^-}j^-(t). \tag{72}$$

Thus, based on (72), the voltage function is given by:

$$V(t) \triangleq \nu_2\left(t, c_{ss}^+(t), c_e^\pm(t,0^\pm), I(t)\right). \tag{73}$$

The function $\nu_2(\cdot)$ indicates the variables on which $V(t)$ depends, showing that the expression is now more compact compared to (13), as it eliminates the dependence on $c_{ss}^-(t)$. As long as (73) is a one-to-one correspondence with respect to $\bar{c}_{ss}^+(t)$, uniformly in $I(t)$, the inversion of voltage function can be derived. As detailed in Remark 2, $c_e^\pm(t,0^\pm)$ can be obtained by measuring related parameters using the EIS technique. Consequently, given access to $c_e^\pm(t,0^\pm)$ and $V(t)$, the surface lithium concentration in the positive electrode $c_{ss}^+(t)$ can be determined as:

$$c_{ss}^+(t) \triangleq \nu_3(t, V(t), c_e^\pm(t,0^\pm), I(t)), \tag{74}$$

where function $\nu_3(\cdot)$ is the inversion of $\nu_2(\cdot)$.

5.2. Solid phase lithium concentration observers

By utilizing the surface particle concentration $c_{ss}^+(t)$, obtained through the inversion of the SPMe voltage function as discussed in Section 5.1, the observer for the solid-phase lithium concentration in the positive electrode (1)–(3) is given as (Moura et al., 2016):

$$\frac{\partial \hat{c}_s^+}{\partial t}(t,r) = D_s^+\left[\frac{2}{r}\frac{\partial \hat{c}_s^+}{\partial r}(t,r) + \frac{\partial^2 \hat{c}_s^+}{\partial r^2}(t,r)\right] + \bar{p}_1^+(r)\left(c_{ss}^+(t) - \hat{c}_{ss}^+(t)\right), \tag{75}$$

$$\frac{\partial \hat{c}_s^+}{\partial r}(t,0) = 0, \tag{76}$$

$$\frac{\partial \hat{c}_s^+}{\partial r}\left(t, R_s^+\right) = \frac{I(t)}{D_s^+ F a_s^+ L^+} + \bar{p}_0^+(t)\left(c_{ss}^+(t) - \hat{c}_{ss}^+(t)\right), \tag{77}$$

where the observer gains are computed as follows:

$$\bar{p}_1^+(r) = \frac{-\lambda D_s^+}{2R_s^+\bar{z}}\left[I_1(\bar{z}) - \frac{2\lambda}{\bar{z}}I_2(\bar{z})\right], \tag{78}$$

$$\bar{p}_0^+ = \frac{1}{2R_s^+}(3-\lambda), \quad \text{for } \lambda < \frac{1}{4}, \tag{79}$$

where $\bar{z} = \sqrt{\lambda\left(\frac{r^2}{\left(R_s^+\right)^2} - 1\right)}$. The observer for the solid-phase lithium concentration in the negative electrode (1)–(3) is given by (Moura et al., 2016):

$$\frac{\partial \hat{c}_s^-}{\partial t}(t,r) = D_s^-\left[\frac{2}{r}\frac{\partial \hat{c}_s^-}{\partial r}(t,r) + \frac{\partial^2 \hat{c}_s^-}{\partial r^2}(t,r)\right] + \bar{p}_1^-(r)\left(c_{ss}^+(t) - \hat{c}_{ss}^+(t)\right), \tag{80}$$

$$\frac{\partial \hat{c}_s^-}{\partial r}(t,0) = 0, \tag{81}$$

$$\frac{\partial \hat{c}_s^-}{\partial r}\left(t, R_s^-\right) = \frac{I(t)}{D_s^- F a_s^- L^-} + \bar{p}_0^-\left(c_{ss}^+(t) - \hat{c}_{ss}^+(t)\right), \tag{82}$$

where observer gains are

$$\bar{p}_0^- = -\frac{a_s^+ L^+ D_s^+}{a_s^- L^- D_s^-}\bar{p}_0^+, \tag{83}$$

$$\bar{p}_1^- = -\frac{a_s^+ L^+}{\left(R_s^+\right)^2 \varepsilon_s^- L^-}\int_0^{R_s^+} r^2 \bar{p}_1^+(r)dr. \tag{84}$$

For solid-phase observer design, it is assumed that $n_{\text{Li,s}}$ is known and the initial condition estimates satisfy

$$n_{\text{Li,s}} = \sum_{i\in\{+,-\}} \frac{\varepsilon_s^i L^i}{\frac{4}{3}\pi (R_s^i)^3}\int_0^{R_s^i} 4\pi r^2 \hat{c}_s^i(0,r)\,dr. \tag{85}$$

If the initial concentration estimates are assumed to be uniform in r, then (85) simplifies to:

$$n_{\text{Li,s}} = \varepsilon_s^+ L^+ \hat{c}_{s,0}^+ + \varepsilon_s^- L^- \hat{c}_{s,0}^-. \tag{86}$$

Theorem 3. *Consider the solid phase lithium concentration PDEs (1)–(3) and designed observers for positive an negative electrodes in (75)–(77) and (80)–(82), respectively. For any initial data $c_{s,0}^{\pm}(\cdot) \in L^2(0, R_s^{\pm})$, the states of the designed observer converges asymptotically to the states of the original system in the spatial L^2 norm if $\hat{c}_s^{\pm}(0,r)$ verifies (86).*

Proof. The stability proof can be found in Theorem 1 of Moura et al. (2016). Note that the surface measurement $c_{ss}^+(t)$ used in the observer is derived as described in Section 5.1, based on electrolyte concentrations at the boundaries and the inversion of the voltage function, which differs from the approach in Moura et al. (2016). □

The estimated SoC, $\widehat{\text{SoC}}(t)$, can be derived by employing $\hat{c}_s^-(t,r)$, obtained from the observer (80)–(82):

$$\widehat{\text{SoC}}(t) = \frac{3}{c_{s,\max}^-}\int_0^1 r^2 \hat{c}_s^-(t,r)\,\mathrm{d}r. \tag{87}$$

Incorporating the boundary electrolyte concentration into the voltage function inversion improves the estimation of $\hat{c}_s^-(t,r)$, resulting in enhanced SoC accuracy.

6. Simulation

To assess the observers' performance, simulations are conducted using the $LiFePO_4$ cell and the UDDS current profile described in Section 3. The electrolyte observers, designed based on the SPMe with modified boundary conditions, are compared against the SPMe with its original boundary conditions (5)–(12), which serves as the truth model. The SPMe model with original boundary conditions has been verified against the Doyle–Fuller–Newman (DFN) model in Moura et al. (2016). Fig. 7 illustrates the error in $c_e^-(t,x)$ between the SPMe with the original and modified boundary conditions. Fig. 8 illustrates the true electrolyte lithium concentration in the negative electrode $c_e^-(t,x)$. In Fig. 8 the electrolyte lithium concentration is initialized at $c_e^-(0,x) = 2$ kmol/m^3, whereas for the observer, the initial condition is set differently as $\hat{c}_e^-(0,x) = 1.1$ kmol/m^3. The boundary measurement $c_e^-(t,0^-)$ is obtained from the electrolyte resistance versus lithium concentration plot derived from EIS experiments in Prada et al. (2012). To account for EIS measurement uncertainty, zero-mean Gaussian noise with a standard deviation of 2% (Lazanas & Prodromidis, 2023) is added to the measurements. The tuning parameter α is chosen as 0.95. For simulation, the PDEs are discretized into ordinary differential equations using the forward finite difference method. In Fig. 9 the estimation error of lithium concentration within the negative electrode $\tilde{c}_e^-(t,x)$ is demonstrated. Initially, a significant error occurs due to different initial conditions, which then decreases and converges over time.

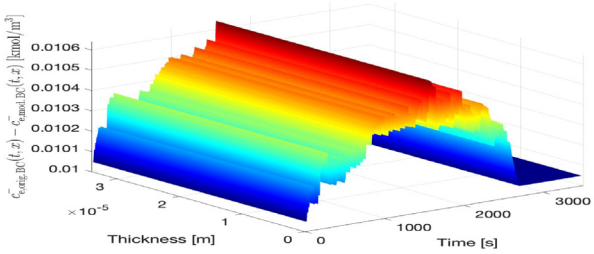

Fig. 7. Error in $c_e^-(t,x)$ between models with original and modified boundary conditions.

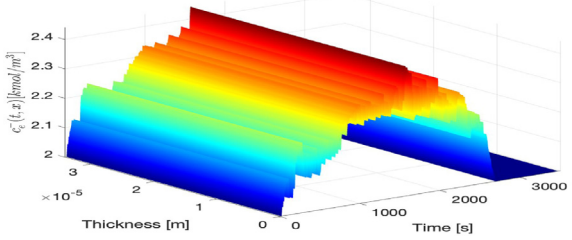

Fig. 8. True electrolyte lithium concentration in the negative electrode $c_e^-(t,x)$.

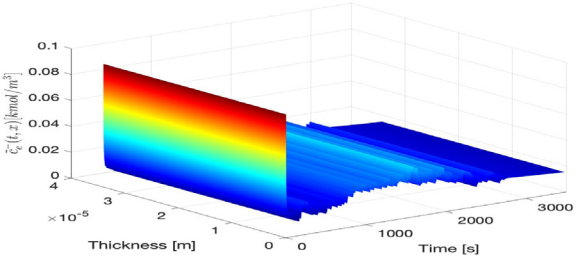

Fig. 9. Estimation error of the electrolyte lithium concentration in the negative electrode $\tilde{c}_e^-(t,x)$.

The estimated electrolyte lithium concentration in the separator is shown in Fig. 10. As evident from the plots, the concentration in the separator region follows a linear trend, aligning perfectly with the quasi-linear assumption used to derive the modified boundary condition. The estimation errors of the lithium

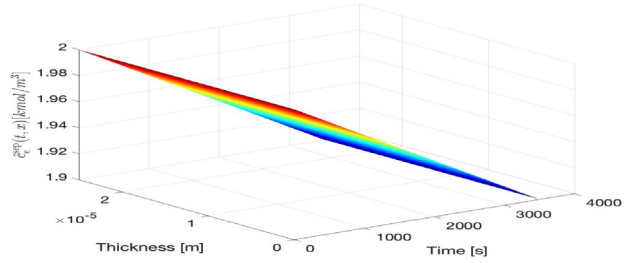

Fig. 10. Estimation of electrolyte lithium concentration in the separator $\hat{c}_e^{sep}(t,x)$.

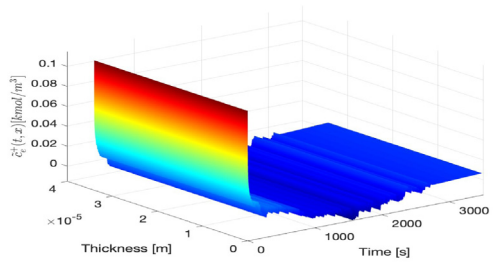

(a)

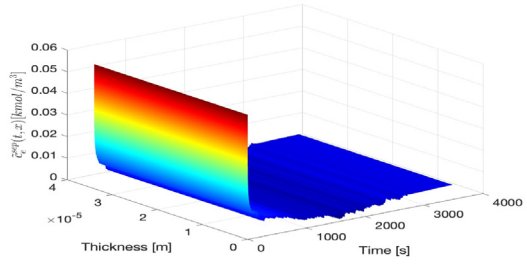

(b)

Fig. 11. Estimation error of electrolyte lithium concentration (a) in the positive electrode (b) in the separator.

concentration in the positive electrode $\tilde{c}_e^{+}(t,x)$ and the separator $\tilde{c}_e^{sep}(t,x)$ are illustrated in Fig. 11(a) and Fig. 11(b), respectively. It can be seen that the error at the initial step quickly diminishes and eventually converges. For the solid-phase lithium concentration simulation, the initial conditions are set as $c_s^{-}(0,r) = 25\,\text{kmol/m}^3$ and $\hat{c}_s^{-}(0,r) = 24.75\,\text{kmol/m}^3$, $\forall r \in [0, 4\times10^{-5}]$ and the tuning parameter λ is set to -0.5. Fig. 12 illustrates the estimation error of the solid-phase lithium concentration in the negative electrode $\tilde{c}_s^{-}(t,r)$, showing convergence over time. Fig. 13 illustrates the comparison between the true SoC and its estimated values. True SoC is the black curve. The blue curve ($\widehat{\text{SoC}}(t)$) shows the SoC estimated using the solid-phase observer, with the boundary condition derived from the inversion of the voltage function, where the electrolyte concentration is estimated using the proposed closed-loop observer in this study. The red curve ($\widehat{\text{SoC}}_{\text{OL}}(t)$) shows the SoC estimated using a solid-phase observer with a boundary condition derived from the inversion of the voltage function, where the electrolyte concentration is estimated using the open-loop observer proposed in Moura et al. (2016). The closed-loop approach yields a more accurate SoC estimation compared to the SoC estimation obtained based on the open-loop observer.

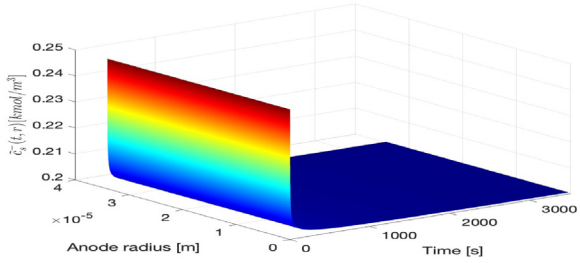

Fig. 12. Solid phase lithium concentration estimation error $\tilde{c}_s^{-}(t,r)$.

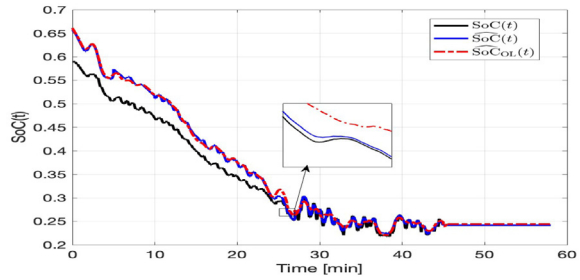

Fig. 13. True SoC(t), estimated SoC using the observer proposed in this study: $\widehat{\text{SoC}}(t)$, and estimated SoC using the observer in Moura et al. (2016): $\widehat{\text{SoC}}_{\text{OL}}(t)$.

7. Conclusion and future works

This paper proposes observers for the lithium concentration in the electrolyte phase using the SPMe with modified boundary conditions. A reverse sensitivity analysis is conducted to identify the most suitable measurement correlated with the electrolyte lithium concentration to find the boundary error. Additionally, by introducing a more reliable inversion of the voltage function, an accurate estimation of solid-phase lithium concentration and SoC is achieved. Finally, simulations are conducted to verify the performance of the proposed schemes. As future work, the original coupled boundary condition could be employed instead of the modified one. Given that EIS is an offline technique, integrating the event-triggered concept (Espitia, Karafyllis, & Krstic, 2021) into the observer offers a potential direction for enhancement. Extending the proposed observer to an adaptive framework to account for aging effects (Moura et al., 2014), as well as incorporating temperature effects (Ferreira & Tang, 2025b), are potential directions for future work. In the simulation analysis, the observers can be applied to a more accurate model, such as the DFN model, and the results compared accordingly.

Acknowledgment

The authors thank Professor Scott Moura for his insights on lithium-ion conservation and its impact on the theoretical developments and simulations in this work.

References

Alipour, Mohammad, Yin, Litao, Tavallaey, Shiva Sander, Andersson, Anna Mikaela, & Brandell, Daniel (2023). A surrogate-assisted uncertainty quantification and sensitivity analysis on a coupled electrochemical–thermal battery aging model. *Journal of Power Sources, 579*, Article 233273.

Baccoli, Antonello, Orlov, Yury, & Pisano, Alessandro (2014). On the boundary control of coupled reaction-diffusion equations having the same diffusivity parameters. In *53rd IEEE conference on decision and control* (pp. 5222–5228). IEEE.

Cerrillo-Gonzalez, María del Mar, Villen-Guzman, M, Vereda-Alonso, Carlos, Rodríguez-Maroto, José Miguel, & Paz-Garcia, Juan Manuel (2022). Acid leaching of $LiCoO_2$ enhanced by reducing agent. Model formulation and validation. *Chemosphere*, *287*, Article 132020.

Chiew, Jia, Chin, Cheng, Toh, W. D., Gao, Zuchang, & Zhang, Caizhi (2019). A pseudo three-dimensional electrochemical-thermal model of a cylindrical $LiFePO_4$ graphite battery. *Applied Thermal Engineering*, *147*, 450–463.

Ecker, Madeleine, Tran, Thi Kim Dung, Dechent, Philipp, Käbitz, Stefan, Warnecke, Alexander, & Sauer, Dirk Uwe (2015). Parameterization of a physico-chemical model of a lithium-ion battery: I. Determination of parameters. *Journal of the Electrochemical Society*, *162*(9), A1836.

Espitia, Nicolás, Karafyllis, Iasson, & Krstic, Miroslav (2021). Event-triggered boundary control of constant-parameter reaction–diffusion PDEs: A small-gain approach. *Automatica*, *128*, Article 109562.

Ferreira, Patryck, & Tang, Shu-Xia (2025a). Cascaded electrochemical-thermal modeling and temperature estimation for cylindrical Li-ion batteries. *Journal of Energy Storage*, *124*, Article 116438.

Ferreira, Patryck, & Tang, Shu-Xia (2025b). Investigating thermal dynamics in cylindrical Li-ion batteries across varied temperatures based on electrochemical principles. *Scientific Reports*, *15*(1), Article 30830.

Jafari, Sadiqa, & Byun, Yung-Cheol (2024). Efficient state of charge estimation in electric vehicles batteries based on the extra tree regressor: A data-driven approach. *Heliyon*.

Karatrantos, Argyrios, Khan, Md Sharif, Yan, Chuanyu, Dieden, Reiner, Urita, Koki, Ohba, Tomonori, et al. (2021). Ion transport in organic electrolyte solutions for lithium-ion batteries and beyond. *Journal of Energy and Power Technology*, *3*(3), 1.

Krstic, Miroslav, & Smyshlyaev, Andrey (2008). Boundary control of PDEs: A course on backstepping designs. SIAM.

Lai, Qingzhi, Jangra, Sidharth, Ahn, Hyoung Jun, Kim, Geumbee, Joe, Won Tae, & Lin, Xinfan (2020). Analytical derivation and analysis of parameter sensitivity for battery electrochemical dynamics. *Journal of Power Sources*, *472*, Article 228338.

Lazanas, Alexandros Ch, & Prodromidis, Mamas I. (2023). Electrochemical impedance spectroscopy A tutorial. *ACS Measurement Science Au*.

Moura, Scott J, Argomedo, Federico Bribiesca, Klein, Reinhardt, Mirtabatabaei, Anahita, & Krstic, Miroslav (2016). Battery state estimation for a single particle model with electrolyte dynamics. *IEEE Transactions on Control Systems Technology*, *25*(2), 453–468.

Moura, Scott J., Chaturvedi, Nalin A., & Krstić, Miroslav (2014). Adaptive partial differential equation observer for battery state-of-charge/state-of-health estimation via an electrochemical model. *Journal of Dynamic Systems, Measurement, and Control*, *136*(1), 011–015.

Newman, John, & Balsara, Nitash P. (2021). *Electrochemical systems*. John Wiley & Sons.

Pesenti, Silvana M. (2022). Reverse sensitivity analysis for risk modelling. *Risks*, *10*(7), 141.

Pesenti, Silvana M., Millossovich, Pietro, & Tsanakas, Andreas (2019). Reverse sensitivity testing: What does it take to break the model? *European Journal of Operational Research*, *274*(2), 654–670.

Prada, Eric, Di Domenico, D., Creff, Yann, Bernard, J., Sauvant-Moynot, Valérie, & Huet, François (2012). Simplified electrochemical and thermal model of $LiFePO_4$-graphite Li-ion batteries for fast charge applications. *Journal of the Electrochemical Society*, *159*(9), A1508.

Rathnayake, Bhathiya, Diagne, Mamadou, Espitia, Nicolás, & Karafyllis, Iasson (2021). Observer-based event-triggered boundary control of a class of reaction–diffusion PDEs. *IEEE Transactions on Automatic Control*, *67*(6), 2905–2917.

Ravikumar, Bharath, Mynam, Mahesh, & Rai, Beena (2018). Effect of salt concentration on properties of lithium ion battery electrolytes: A molecular dynamics study. *The Journal of Physical Chemistry C*, *122*(15), 8173–8181.

Schmidt, Alexander P., Bitzer, Matthias, Imre, Árpád W., & Guzzella, Lino (2010). Experiment-driven electrochemical modeling and systematic parameterization for a lithium-ion battery cell. *Journal of Power Sources*, *195*(15), 5071–5080.

Sepasiahooyi, Sara, & Tang, Shu-Xia (2024a). Enhanced battery state estimation: Part 1. Electrolyte lithium-ion concentration observer. In *Conference on decision and control*. IEEE.

Sepasiahooyi, Sara, & Tang, Shu-Xia (2024b). Enhanced battery state estimation: Part 2. Reverse sensitivity analysis and electrode lithium-ion observer. In *Conference on decision and control*. IEEE.

Sepasiahooyi, Sara, & Tang, Shu-Xia (2024c). Sensitivity analysis of lithium-ion battery SoH indicators: An analytical study. In *American control conference, 2024*. IEEE.

Tang, Shu-Xia, Camacho-Solorio, Leobardo, Wang, Yebin, & Krstic, Miroslav (2017). State-of-Charge estimation from a thermal–electrochemical model of lithium-ion batteries. *Automatica*, *83*, 206–219.

Xu, Jianing, Wang, Tiansi, Pei, Lei, Mao, Shitong, & Zhu, Chunbo (2020). Parameter identification of electrolyte decomposition state in lithium-ion batteries based on a reduced pseudo two-dimensional model with Padé approximation. *Journal of Power Sources*, *460*, Article 228093.

Zhang, Dong, Couto, Luis D., & Moura, Scott J. (2020). Electrode-level state estimation in lithium-ion batteries via Kalman decomposition. *IEEE Control Systems Letters*, *5*(5), 1657–1662.

Zhang, Dong, Park, Saehong, Couto, Luis D., Viswanathan, Venkatasubramanian, & Moura, Scott J. (2022). Beyond battery state of charge estimation: Observer for electrode-level state and cyclable lithium with electrolyte dynamics. *IEEE Transactions on Transportation Electrification*.

Sara Sepasiahooyi is currently a Ph.D. student in Mechanical Engineering at Texas Tech University, USA. She received her M.S. degree in Electrical Control Engineering from Amirkabir University of Technology (Tehran Polytechnic), Iran, and her B.S. degree in Electrical Control Engineering from Shariati Technical University, Iran. Her current research focuses on state estimation of lithium-ion battery systems, with an emphasis on fault diagnosis, aging modeling, and distributed parameter systems.

Shu-Xia Tang received her Ph.D. in Mechanical Engineering in 2016 from the Department of Mechanical & Aerospace Engineering, University of California, San Diego, USA. She is currently an assistant professor at the Department of Mechanical Engineering, Texas Tech University, USA. She is an IEEE senior member and the founding chair of ASME (American Society of Mechanical Engineers) Technical Committee on Distributed Parameter Systems (DPS). She serves on the IEEE CSS (Control Systems Society) Technical Committee on DPS, IFAC Technical Committee on DPS, ASME Technical Committee on Energy Systems, ASME Technical Committee on Automotive & Transportation Systems, ASME Technical Committee on Vibrations. She serves as an editorial team member of the IFAC Technical Committee on DPS and an Editorial Board member of IEEE CSS and ASME DSCD. She served on the editorial team of ASME Dynamic Systems and Control Division (DSCD) Newsletter, 2021–2024, and served as the associate editor of Journal of Control, Automation and Electrical Systems, 2018–2022. Her main research interests are stability analysis, estimation and control design of distributed parameter systems including swarm robotic systems and energy storage systems.